UC Berkeley
UC Berkeley Previously Published Works

Title

Excitation functions and isomeric cross-section ratios of (d,xn) reactions on 86Sr

Permalink

Journal

The European Physical Journal A, 60(6)

ISSN

1434-6001

Authors

Uddin, Md Shuza

Sudár, Sándor

Basunia, M Shamsuzzoha

et al.

Publication Date

2024

DOI

10.1140/epja/s10050-024-01330-6

Copyright Information

Peer reviewed

THE EUROPEAN
PHYSICAL JOURNAL A

Excitation functions and isomeric cross-section ratios of (d,xn) reactions on ^{86}Sr

Md. Shuza Uddin[1,2,3], **Sándor Sudár**[4], **M. Shamsuzzoha Basunia**[2], **Bernhard Scholten**[1], **Stefan Spellerberg**[1], **Andrew S. Voyles**[2,6], **Jonathan T. Morrell**[2], **Ingo Spahn**[1], **Alex Hermanne**[5], **Lee A. Bernstein**[2,6], **Bernd Neumaier**[1], **Syed M. Qaim**[1,a]

[1] Institut für Neurowissenschaften und Medizin, INM-5: Nuklearchemie, Forschungszentrum Jülich, 52425 Jülich, Germany
[2] Nuclear Science Division, Lawrence Berkeley National Laboratory, Berkeley, CA 94720, USA
[3] Tandem Accelerator Facilities, INST, Atomic Energy Research Establishment, Savar, Dhaka, Bangladesh
[4] Institute of Experimental Physics, University of Debrecen, 4010 Debrecen, Hungary
[5] Cyclotron Laboratory, Vrije Universiteit Brussel (VUB), 1090 Brussels, Belgium
[6] Department of Nuclear Engineering, University of California, Berkeley, CA 94720, USA

Abstract Excitation functions of the ^{86}Sr(d,n)^{87m,87g}Y, ^{86}Sr(d,2n)^{86m,86g}Y and ^{86}Sr(d,3n)^{85m,85g}Y reactions on enriched ^{86}Sr target were measured by the activation technique up to deuteron energies of 49 MeV. The isomeric cross-section ratios as a function of projectile energy were deduced from the measured data for ^{87m}Y, ^{87g}Y(cum), ^{86m}Y, ^{86g}Y(cum), ^{85m}Y and ^{85g}Y pairs for the same energy range. All measurements are reported for the first time. The experimental data were compared with the data from the TENDL library which is based on TALYS calculation with default parameters. No satisfactory agreement was observed. Nuclear model calculations were then performed using the codes TALYS and EMPIRE with some parameter adjustments, and compared with the experimental data. The quality of the agreement between experimental data and model calculations was numerically quantified. In general, the data as well as the isomeric cross-section ratios are partially reproduced by the model calculations, provided the input model parameters are properly chosen and the level structure of the product nucleus is thoughtfully considered.

1 Introduction

Studies of excitation functions of charged-particle induced reactions are important for testing nuclear models as well as for practical applications. Over the last three decades, extensive experimental work has been performed worldwide on reaction products induced by light charged particles, mainly protons of energies up to about 30 MeV, but also extending in some cases up to 100 MeV and beyond cf. [1]. However, since many of the measurements were done on targets of natural isotopic composition, the activation cross sections obtained were found to be of limited use in assuring the desired radionuclidic purity of the investigated radionuclide, or for a rigorous testing of nuclear models. For the latter, it is important to use monoisotopic targets which restrict the number of reaction channels leading to the formation of a certain product. A continuous programme has been underway at the Forschungszentrum Jülich (FZJ) to perform experiments using monoisotopic elements or highly enriched isotopes as targets in various mass regions to study reactions induced by protons, deuterons, ^{3}He- and α-particles of energies up to 40 MeV and nuclear model calculations were performed using several codes in cooperation with theorists in Vienna and Debrecen cf. [2–10]. In recent years, several other laboratories, e.g. in Nantes, Legnaro, Warsaw, Berkeley, Los Alamos, etc., have also got actively engaged in detailed measurements using monoisotopic and enriched targets combined with extensive nuclear modelling cf. [11–17], mostly with protons, but to a limited extent also with deuterons and α-particles. The need of proper choice of input model parameters for describing the excitation function has been often emphasized.

Very recently we described a study under an international collaboration on the interaction of protons with ^{86}Sr, measuring cross sections of the ^{86}Sr(p,n)$^{86g+xm}$Y reaction [18], for which the available database was discrepant. This reaction is commonly used for the production of ^{86g}Y (T$_{1/2}$ = 14.7 h) which constitutes a positron-emitting diagnostic partner of

Springer

the β^--emitting therapeutic radionuclide ^{90}Y (T$_{1/2}$ = 2.7 d) in theranostic studies. The kinetic data obtained via a positron emission tomographic (PET) measurement using ^{86g}Y allow to quantify the radiation dose in the internal radionuclide therapy with ^{90}Y [19,20]. Our new data solved the discrepancies in cross sections and the theoretically calculated yield of ^{86g}Y agreed with the result of experimental yield measurement. Furthermore, attention was also paid to the formation of the isomeric states in ^{86m,g}Y and ^{85m,g}Y [21] which constituted two interesting even/odd mass neighbouring nuclei, because the spins of the nuclear levels concerned differ considerably and the modes of decay of the isomeric states in the two cases are different. In general, the nuclear model calculations were fairly successful in describing both experimental cross sections and isomeric cross-section ratios, provided the input parameters were carefully chosen. In particular, the effect of η, which is related to the spin distribution of the level density, on the isomeric cross-section ratio was investigated in detail.

The present work describes investigations on deuteron induced reactions on enriched ^{86}Sr, similar to the ones mentioned above for protons. There were two motivations: (a) to determine cross sections for the formation of ^{87m,g}Y, ^{86m,g}Y and ^{85m,g}Y for applications. For the production of ^{86g}Y for theranostic application (see above), several routes, e.g. ^{86}Sr(p,n)^{86g}Y, ^{88}Sr(p,3n)^{86g}Y, ^{nat}Rb(^{3}He,xn)^{86g}Y, ^{nat}Zr(p,x)^{86g}Y, etc., have been investigated cf. [20], but not the ^{86}Sr(d,2n)$^{86g+xm}$Y reaction. Since in the production of several radionuclides the (p,n) and (d,2n) reactions are often competitive, provided the level of radioactive impurities can be controlled, we considered it important to perform the measurements. Although in irradiation of ^{86}Sr with deuterons several radioisotopes of Sr and Rb (e.g. ^{85}Sr, ^{84}Rb, ^{83}Rb, etc.) are also formed as impurities, they are easily removed by a chemical separation [20]. The isotopic impurities of ^{86g}Y, namely ^{85m,g}Y and ^{87m,g}Y, however, can only be controlled by a proper choice of nuclear data. Our new data should therefore help the radioisotope producers to decide whether the (d,2n) process on ^{86}Sr could lead to ^{86g}Y of the same quality as the (p,n) reaction. (b) to test the predictive power of nuclear model calculations. It is known that the modelling of the activation products formed in the interactions of deuterons with target nuclei is more challenging cf. [22–25]. The (d,2n) and (d,3n) reaction cross sections show some systematics. The description of the (d,n) process, however, is problematic. Here we present the first experimental data for deuterons on enriched ^{86}Sr up to 50 MeV. The results of model calculations using both default parameters and some parameter adjustments are also reported in an attempt to explain the experimental data. In the literature, except for a measurement of deuterons on ^{nat}Sr [26], no data relevant to the present study are available.

2 Experimental

2.1 Sample preparation and irradiations

Excitation functions of deuteron-induced reactions on enriched ^{86}Sr were measured by the stacked-sample activation technique. The enriched ^{86}Sr material was provided as ^{86}SrCO$_3$ powder (isotopic composition: 96.4% ^{86}Sr; 1.33% ^{87}Sr; 2.26% ^{88}Sr; supplied by Eurisotop, France). Thin strontium carbonate samples were prepared at the Forschungszentrum Jülich (FZJ) by the sedimentation technique, the details of which have been given in our earlier study on the proton-induced nuclear reactions on ^{86}Sr [18,21]. A 50 μm thick Al foil (supplied by Goodfellow; chemical purity: 99.0%) was used as the backing for sedimentation. The sedimented layers were examined under a microscope and only homogeneous and mechanically stable samples were selected. The exact diameter of each deposit was determined through the analysis of a photograph of the sediment [18]. The net weight of the sediments lay in the range of 5 to 7 mg. Each sedimented sample was then covered by a 10 μm thick Al foil of 16 mm diameter, welted around the backing foil.

Thin foils of Al, Ti, Fe and Cu of natural isotopic composition (supplied by Goodfellow, purity: Al (99.0%); Ti (>99.6%); Fe(99.6%); Cu (99.9%), thickness of both Fe and Ti foils; 25 μm, Al foil; 50 and 250 μm, Cu foil; 50 μm) were used as beam monitors and inserted into the stack to follow the beam energy distribution as well as the beam parameters along the stack. Each foil was cut in circular disc with a diameter of 13 mm. Four stacks were prepared with ^{86}SrCO$_3$ sediment samples together with the monitor foils for irradiations with the deuteron beam.

One stack containing ^{86}Sr-targets was irradiated with deuterons of primary energy 33 MeV and the other one with 40 MeV, for 30 and 45 min, respectively, at the 88 Inch Cyclotron, Lawrence Berkeley National Laboratory (LBNL), USA. In both of the irradiations, the beam current was kept constant at approximately 100 nA. Two other stacks were irradiated with 50 MeV primary energy deuterons using the external beam of the CGR930 cyclone Cyclotron of the Université Catholique in Louvain-la-Neuve, Belgium. Each irradiation was performed for 30 min, and the beam current was kept constant at approximately 200 nA.

2.2 Energy and flux of deuterons

The extracted beams at the 88 Inch Cyclotron at LBNL as well as at the CGR930 cyclotron in Louvain-la-Neuve are well characterized. The energy of the extracted deuteron beam was given by the accelerator parameters. The mean energy of the deuteron beam effective in the front Cu foil was confirmed by comparing the experimentally obtained decay-rate ratio of ^{62}Zn/^{63}Zn formed in the same monitor foil

with the value calculated theoretically from the IAEA recommended excitation functions of the reactions $^{nat}Cu(d,x)^{62}Zn$ and $^{nat}Cu(d,x)^{63}Zn$, respectively [27]. More details of the method have been reported earlier [28,29].

The irradiation of the monitor foils Al, Ti, Fe and Cu, placed in front of a stack, led to the monitor reactions $^{27}Al(d,x)^{24}Na$, $^{nat}Ti(d,x)^{48}V$, $^{nat}Fe(d,x)^{56}Co$ and $^{nat}Cu(d,x)^{62,63}Zn$, respectively. The deuteron flux was determined from the measured decay rates of ^{24}Na, ^{48}V, ^{56}Co and $^{62,63}Zn$ at the end of bombardment (EOB) and the reference cross section of the respective monitor reaction taken from the IAEA evaluated data file [27]. The individual flux values from the above monitors agreed with one another within 5%. An average of those values was used to determine the cross section of the investigated reaction. This flux value was considered nearly constant in the stack. The excitation function of each monitor reaction was measured to adjust the beam energy in the stack. The measured excitation functions reproduced well the recommended curves given by the IAEA [27]. This added high confidence to the various techniques used in our measurements. As an example, the measured excitation function of the monitor reaction $^{27}Al(d,x)^{24}Na$, has been reported in [25]. The computer program, STACK, written at FZJ and based on the energy-range relation [30], was utilized to calculate the beam energy degradation along the stack.

2.3 Measurement of radioactivity and analysis

The radioactivity of a reaction product in the activated foil or sample was measured non-destructively using high-purity germanium (HPGe) detector γ-ray spectrometry. The detector was associated with the necessary electronics and Maestro data acquisition software. The radioactivity measurements were carried out at three facilities: (i) FZJ, Germany, (ii) VUB, Brussels, Belgium, and (iii) LBNL, USA. The energy resolutions (FWHM) at 1332.5 keV of ^{60}Co of the HPGe detectors used were 1.9 keV at FZJ, 1.9 keV at VUB and 2.5 keV at LBNL. For efficiency calibration of the detectors, standard point sources were used: at LBNL ^{54}Mn, ^{133}Ba, ^{137}Cs and ^{152}Eu, supplied by Isotope Products Laboratories, at FZJ ^{22}Na, ^{54}Mn, ^{57}Co, ^{60}Co, ^{88}Y, ^{137}Cs, ^{152}Eu, ^{226}Ra and ^{241}Am, supplied by Eckert & Ziegler, Berlin, and at VUB ^{60}Co, ^{137}Cs and ^{152}Eu, supplied by LMSI, Coffret D'Etalons BETA ECBU. The uncertainty in the activity of each source was specified as 3%. The γ-ray spectra measured in this work were analyzed by both the GammaVision and FitzPeaks [31] software. The counting was done repeatedly in several time segments depending on the half-life of the radionuclide. Measurements were carried out at a distance of 5 cm, 10 cm, 20 cm, 40 cm or 50 cm from the surface of the detector. The decay data of the investigated radionuclides were taken from the Lund/LBNL Nuclear Database [32] and some recent references [33,34]; they are collectively given in Table 1.

At LBNL, USA, the short-lived ^{86m}Y ($T_{1/2}$ = 47.4 min) activity was measured within 1 to 4 h after EOB at a distance of 50 cm. It was identified by its characteristic γ-ray of energy 208 keV. The radioactivity of each of the two radionuclides ^{85m}Y ($T_{1/2}$ = 4.86 h) and ^{85g}Y ($T_{1/2}$ = 2.68 h) was measured at a distance of 20 cm. The ^{85m}Y mainly decays to ^{85}Sr through β^++EC processes, and its isomeric decay ($< 0.002\%$) to the ground state ^{85g}Y is negligible. The ^{85m}Y activity was assessed by its characteristic gamma line at 535.6 (3.46%) keV. It was also checked by measurement of other three weak gamma lines at 767.3 (3.6%), 768.6 (1.3%) and 769.7 (0.3%) keV as a triplet. For measurement of the ^{85g}Y activity, the 504 keV γ-line was used. It was located close to the 511 keV annihilation peak, with partial overlapping. Using the FitzPeak gamma analysis software [31], net peak area of the 504 keV line could be determined conveniently. The third step of counting was devoted to the measurement of the ^{86g}Y radioactivity after the complete decay of ^{86m}Y ($T_{1/2}$ = 47.4 min) to the ground state, and the ^{87m}Y radioactivity. The last step of measurement of each sample was related to the determination of the radioactivity of the long-lived product ^{87g}Y.

After irradiation at the CGR930 cyclotron in Louvain-la-Neuve, the radioactive samples were transferred by special transport to the Cyclotron Laboratory, VUB, Brussels, Belgium, about 20 km away from Louvain-la-Neuve, where the activity of the short-lived radionuclides $^{85m,85g}Y$ and ^{86m}Y was determined. Measurement was started about three hours after EOB at a distance of 20 cm from the detector surface to keep the dead time below 5%. The irradiated samples were thereafter transferred by special transport to the Nuclear Chemistry Laboratory of the Forschungszentrum Jülich (FZJ), Germany, about 200 km away from Brussels. Measurement at FZJ was started one day after EOB; thus the metastable state ^{86m}Y ($T_{1/2}$ = 47.4 min) had completely decayed to ^{86g}Y before measuring the activity. The ^{86g}Y ($T_{1/2}$ = 14.7 h) and ^{87m}Y ($T_{1/2}$ = 13.4 h) radioactivities were measured for 1 h at a distance of 20 cm. Due to a complicated level scheme with numerous coincident transitions, the effect of true coincident gamma ray summing for the analyzed gammas of ^{86g}Y was not negligible at 20 cm distance. Therefore corrections for coincident summing were calculated with the TrueCoinc program [35]. Similarly, the ^{87g}Y activity was measured after disappearance of the 380.8 keV peak of the metastable state ^{87m}Y ($T_{1/2}$ = 13.4 h) in the spectrum, i.e. about a week after EOB at a distance of 5 cm for 4–16 h to obtain good statistics. Each sample was counted 3–4 times by giving sufficient decay interval to check the half-lives of the activation products as well as to avoid interference by overlapping γ-lines from undesired products.

Table 1 Decay data[a] and production routes of the investigated radionuclides in irradiations of enriched ^{86}Sr with deuterons of energies up to 50 MeV

Radionuclide	Spin	Decay mode (%)	Half-life	γ-ray energy (keV)	γ-ray intensity (%)	Production route	Q-value (MeV)
^{85m}Y	$(9/2)^+$	$\beta^+ = 57$ EC=43	4.86(13) h	535.6 767.3	3.46(29) 3.6(5)[c]	^{86}Sr(d,3n) ^{87}Sr(d,4n)[d] ^{88}Sr(p,5n)[d]	−17.78 −26.21 −37.32
^{85g}Y	$(1/2)^-$	$\beta^+ = 66$ EC = 34	2.68(5) h	504.44 913.89	60(2) 9.0(9)	^{86}Sr(d,3n) ^{87}Sr(d,4n)[d] ^{88}Sr(p,5n)[d]	−17.76 −26.19 −37.30
^{86m}Y	$(8)^+$	IT = 99.31 EC = 0.25 $\beta^+ = 0.44$	47.4(4) min	208.1	93.8 (9)	^{86}Sr(d,2n) ^{87}Sr(d,3n)[d] ^{88}Sr(d,4n)[d]	−8.46 −16.89 −28.01
^{86g}Y[b]	4^-	$\beta^+ = 27$ EC = 73	14.74(2) h	442.8 443.7 627.7 1152.8	15.4(5) 0.80(2) 32.6(10) 30.5(9)	^{86}Sr(d,2n) ^{87}Sr(d,3n)[d] ^{88}Sr(d,4n)[d]	−8.25 −16.68 −27.79
^{87m}Y	$9/2^+$	IT = 98.43 EC = 1.57	13.37(3) h	380.8	78.0(1)	^{86}Sr(d,n) ^{87}Sr(d,2n)[d] ^{88}Sr(d,3n)[d]	3.18 −5.25 −16.36
^{87g}Y	$1/2^-$	EC = 99.82 $\beta^+ = 0.18$	79.8(3) h	388.53 484.8	82.2(7) 89.8(9)	^{86}Sr(d,n) ^{87}Sr(d,2n)[d] ^{88}Sr(d,3n)[d]	3.56 −4.87 −15.98

[a] Decay data taken from references [32,36,37], unless otherwise stated
[b] Taken from recent references [33,34]
[c] This is for a triplet peak (see text)
[d] This reaction occurs on the respective low-abundant impurity target isotope present in the enriched ^{86}Sr target

2.4 Reaction cross section and its uncertainty

The net area under a peak of the characteristic γ-ray of an investigated radionuclide was converted to count rate and extrapolated to the end of bombardment (EOB). The count rate at EOB was converted to the decay rate by applying the necessary corrections for γ-ray intensity, efficiency of the detector and true coincidence losses, if any. From the decay rate at EOB and the deuteron beam intensity measured by activation of the monitor foils, the cross section for the formation of a product radionuclide could be determined using the well-known activation formula.

The contribution to the reaction product from subsidiary reactions on the undesired target isotopes ^{87}Sr (1.33%) and ^{88}Sr (2.26%) present in the enriched ^{86}Sr target was significant in the case of ^{87}Y production. In this case, the corrections were based on Eq. A11 in the Appendix, using Tárkányi et al. [26] experimental data on the natural composition target, which contains (82.58%) ^{88}Sr. The correction for ^{87}Sr was based on TALYS calculations using the same optical model parameters (OMP) and level schema as those used for the ^{86}Sr target. While the energy grid of Tárkányi et al. [26] was different from ours, their data and the uncertainty were interpolated to our energy grid. The details on the correction are summarized in Table 2. It shows the ratio of the corrected to uncorrected data, but the corrections are based on subtract-

ing the contributions of ^{87}Sr and ^{88}Sr. The contribution of the model-based correction is, on average (5%) and above 40 MeV deuteron energy, it is even less, only (3%). The uncertainty of Tárkányi's measurement and a (20%) uncertainty for the model calculation were taken into account in the final uncertainty data using the usual error propagation law.

We want to mention that the corrections were calculated by Eq. A7 in the Appendix as well. It uses a ratio of model-calculated data to get a correction factor. This method has given quite similar results, and some viewpoints seemed better, for example, the smoother connection of the two independent measurement sets between 30 and 40 MeV in the case of the ^{86}Sr(d,n)$^{87(g+xm)}$Y reaction. In the case of the ^{86}Sr(d,2n) and ^{86}Sr(d,3n) reactions the Eq. A7 of the Appendix was used for correction. Their values for the ^{86}Sr(d,2n) and ^{86}Sr(d,3n) reactions were on average(5%) and (1%), respectively.

The overall uncertainty in the cross section was obtained by summing in quadrature the individual uncertainties in: counting statistics (0.4–10%), efficiency of the detector (4%), true coincidence correction (< 2%), γ-ray intensities (0.1–5%), half-life (0.2 to −2.67%), deuteron flux (6%) and sample homogeneity (up to 5%). The overall uncertainties of the measured cross sections are (between 8 and 14%)(1σ), including (5%) uncertainty in the estimation of the contri-

bution of the subsidiary reactions deduced from the nuclear model calculations.

The uncertainty of the isomeric ratio was estimated from the individual uncertainties in counting statistics, detector efficiency, γ-ray intensity and half-life of both the metastable state and the ground state. While dividing the formula for the cross sections of metastable state and ground state, the common parameters like flux of deuterons and weight of the sample, were eliminated. The uncertainty in the isomeric cross-section ratio was thus smaller and amounted to 5–7%. For the ^{85m,g}Y pair we calculated σ_m/σ_g, i.e., the ratio of the directly measured values and not σ_m/σ_{m+g}. The associated uncertainty was about 11% and thus comparatively higher

Table 2 Measured cross sections for the production of ^{87}Y via the ^{86}Sr+d process[a]

Deuteron energy (MeV)	Labora-tory	^{87m}Y σ (mb)	^{87m}Y$_{unc}$ σ (mb)	Corr. fact.	^{87}Sr cal-th (%)	$^{87(g+xm)}$Y[b] σ (mb)	$^{87(g+xm)}$Y[b]$_{unc}$ σ (mb)	Corr. fact.	^{87}Sr cal-th (%)
49.1 ± 0.3	FZJ	22.8 ± 3.0	29.7 ± 2.9	0.77	2.0	25.3 ± 3.5	36.4 ± 3.3	0.70	3.0
47.9 ± 0.3		22.4 ± 2.9	29.1 ± 2.8	0.77	2.3	26.4 ± 3.6	37.6 ± 3.4	0.70	3.2
46.7 ± 0.3		24.3 ± 3.3	32.4 ± 3.1	0.75	2.4	35.7 ± 4.6	48.7 ± 4.4	0.73	2.8
45.5 ± 0.3		23.5 ± 3.3	32.3 ± 3.1	0.73	2.5	34.8 ± 4.7	49.0 ± 4.4	0.71	2.9
44.3 ± 0.3		22.7 ± 3.2	31.6 ± 3.1	0.72	2.9	36.7 ± 4.9	51.6 ± 4.6	0.71	3.1
43.0 ± 0.4		20.5 ± 3.0	29.5 ± 2.9	0.70	3.4	34.1 ± 4.6	48.5 ± 4.4	0.70	3.7
41.7 ± 0.4		18.9 ± 2.9	28.5 ± 2.8	0.66	3.8	34.1 ± 4.6	48.8 ± 4.4	0.70	4.0
40.4 ± 0.4		22.8 ± 3.5	34.0 ± 3.3	0.67	3.6	42.0 ± 5.6	59.0 ± 5.3	0.71	3.6
38.9 ± 0.4		19.3 ± 3.4	32.1 ± 3.1	0.60	4.2	38.1 ± 5.6	58.1 ± 5.2	0.66	4.1
36.2 ± 0.4		24.7 ± 4.3	40.9 ± 4.0	0.60	3.9	45.3 ± 6.8	70.1 ± 6.3	0.65	4.0
36.0 ± 0.4		23.6 ± 4.3	40.2 ± 3.9	0.59	4.1	44.6 ± 6.8	69.7 ± 6.3	0.64	4.1
33.1 ± 0.5		27.4 ± 5.2	48.5 ± 4.7	0.57	3.9	49.2 ± 8.2	82.5 ± 7.4	0.60	4.1
32.9 ± 0.5		24.9 ± 5.0	46.2 ± 4.5	0.54	4.2	49.6 ± 8.2	83.0 ± 7.5	0.60	4.1
30.1 ± 0.5		18.4 ± 4.7	41.9 ± 4.1	0.44	5.5	40.1 ± 7.7	75.3 ± 6.8	0.53	5.3
36.9 ± 0.3	LBNL	14.9 ± 3.1	30.1 ± 2.7	0.50	5.0	31.2 ± 5.4	54.9 ± 4.8	0.57	4.9
34.1 ± 0.3		15.1 ± 3.7	34.8 ± 3.1	0.43	5.3	41.9 ± 7.1	72.6 ± 6.4	0.58	4.4
31.1 ± 0.3		14.6 ± 4.1	37.6 ± 3.4	0.39	5.7	41.6 ± 7.6	76.2 ± 6.7	0.55	5.0
28.2 ± 0.3		5.6 ± 3.6	29.7 ± 2.7	0.19	8.6	30.6 ± 6.9	66.8 ± 5.9	0.46	6.7
28.1 ± 0.4		10.9 ± 3.9	34.9 ± 3.1	0.31	7.4	34.0 ± 7.2	70.1 ± 6.2	0.49	6.4
24.6 ± 0.4		6.6 ± 3.3	28.4 ± 2.5	0.23	12.3	22.0 ± 6.0	56.5 ± 5.0	0.39	10.5
21.7 ± 0.4		22.8 ± 3.9	39.7 ± 3.5	0.57	12.6	57.9 ± 8.0	85.7 ± 7.5	0.68	9.7
20.9 ± 0.4		22.3 ± 3.8	38.3 ± 3.4	0.58	14.4	65.6 ± 8.5	91.7 ± 8.1	0.72	9.9
18.5 ± 0.4		33.6 ± 4.2	44.7 ± 3.9	0.75	15.0	85.2 ± 9.4	103 ± 9	0.83	10.7
16.9 ± 0.4		55.7 ± 5.9	65.2 ± 5.7	0.86	10.4	131 ± 13	146 ± 13	0.90	7.6
15.2 ± 0.4		56.1 ± 5.9	64.7 ± 5.7	0.87	10.1	124 ± 12	138 ± 12	0.90	7.8
13.4 ± 0.5		73.6 ± 7.2	81.1 ± 7.1	0.91	7.4	166 ± 16	179 ± 16	0.93	5.5
11.4 ± 0.5		119 ± 11	125 ± 11	0.95	4.0	257 ± 24	267 ± 23	0.96	3.0
10.5 ± 0.5		244 ± 22	249 ± 22	0.98	1.7	525 ± 47	532 ± 47	0.99	1.3
10.1 ± 0.5		366 ± 33	370 ± 33	0.99	1.1	772 ± 68	777 ± 68	0.99	0.8
7.9 ± 0.5		116 ± 11	118 ± 11	0.99	1.2	311 ± 28	313 ± 28	0.99	0.7
6.2 ± 0.5		48.6 ± 4.4	48.7 ± 4.4	1.00	0.2	201 ± 18	201 ± 18	1.00	0.1

[a] In spite of the enriched target, containing 96.4% of ^{86}Sr, the small amount of ^{87}Sr and ^{88}Sr cause significant contribution to ^{87}Y. The corrections were done using Eq. A11, utilizing Tárkányi et al. [26] measurements on the natural composition target, which contains the ^{88}Sr in 82.58%. The correction for the ^{87}Sr was based on the TALYS calculations using the same optical model parameters (OMP) model and same level schema as used for ^{88}Sr target. The unc label means the uncorrected cross section data (i.e. including the production caused by the ^{87}Sr and ^{88}Sr). The column "Corr. fact." contains the ratio of the corrected and uncorrected cross sections, while the column "^{87}Sr cal-th " shows the contribution of the TALYS calculation based correction in percent. To get the effective cross section for this isotopic composition, the uncorrected cross section has to be multiplied by 0.964

[b] Cumulative cross section (g+xm) of a product describes the sum of its independent formation as well as via the decay of the metastable state

due to uncertainty inferred from the gamma-ray intensity and half-life of ^{85m}Y.

3 Nuclear model calculations

The reaction cross sections were calculated using the nuclear model code TALYS [38] version 1.9, adopting an equidistant excitation energy grid. TALYS incorporates several nuclear models to analyze all the significant nuclear reaction mechanisms over the energy range of 1 keV to 200 MeV. In the calculations, the particle transmission coefficients were generated via the spherical optical model using the ECIS-06 code [39] with global parameters: for neutrons and protons from Koning et al. [40]; for the OMP of complex particles (d, t, ^{3}He) the code made use of a folding approach, building up the OMPs from the neutron and proton potential. For the OMP of alpha particles, instead of the TALYS default parameter set of Avrigeanu et al. [41] the folding approach of TALYS was used because it can be adjusted to the experimental data. The OM parameters for deuteron, protons, and neutrons were modified to get the best description of the experimental data. The gamma-ray transmission coefficients were calculated through the energy-dependent gamma-ray strength function according to Kopecky and Uhl [42] for E1 radiation, and according to Brink [43] and Axel [44] for all the other transition types. For the pre-equilibrium reactions, a two-component exciton model of the TALYS code was used. The energies, spins, parities, and branching ratios of the discrete levels were based on the RIPL-3 database [45]. In some cases, the energies, spins, parities, and branching ratios of the discrete levels were modified based on the information in Ref. [36]. In the continuum region, the level density was calculated by the back-shifted Fermi gas model (BSFG) [46], using its slightly modified version in TALYS [40]. For the ratio of the effective moment of inertia to the rigid body moment of inertia parameter of the spin distribution of the level density (η), the systematics based on the evaluation by Sudár and Qaim [10] was used. Regarding discrete levels, it is known that their influence on the calculated isomeric cross-section ratio is very strong. In the case of ^{86}Y, the properties of the low-lying levels and gamma transitions are either not known or known poorly. Many of these missing/tentative data are simply assumed and made available in the TALYS input based on RIPL [45]. In our previous work [21] we dealt with different options for the assumed properties to reproduce proton-induced reaction cross sections, and the same level scheme was also used in this work.

Our aim was to compare the different reaction model codes which emphasize the direct processes and the isomeric cross sections, and their database of the input parameters. The second selected code was EMPIRE [47] which is also quite successful. EMPIRE is also a modular system of nuclear reaction codes, comprising various nuclear models, and designed for calculations over a broad range of energies and incident particles. The code accounts for the major nuclear reaction models, such as the optical model, Coupled Channels and DWBA (ECIS06 and OPTMAN), Multistep Direct (ORION + TRISTAN), NVWY Multi-step Compound, exciton model (PCROSS), hybrid Monte Carlo simulation (DDHMS), and the full-featured Hauser-Feshbach model including width fluctuations and the optical model for fission. A comprehensive library of input parameters based on the RIPL-3 library covers nuclear masses, optical model parameters, ground state deformations, discrete levels and decay schemes, level densities, fission barriers, and γ-ray strength functions. The properly parametrized Enhanced Generalized Superfluid Model (EGSM) (including adjustment to discrete levels) is the default level density formulation in the EMPIRE code; therefore, it is also referred as 'Empire Global Specific Model'. The EGSM uses, as GSM, the super-fluid model below critical excitation energy and the Fermi Gas model above. Enhancement compared to GSM relates mainly to the spin distribution in the Fermi Gas model. During the calculation, the EMPIRE-specific level densities were selected. Exciton model calculations were performed with the PCROSS code. Cluster emission utilized parametrization of the Iwamoto-Harada model. The mean free path parameter in PCROSS was set to the recommended 1.5 value. Gamma emission width is not normalized. Optical model parameters for neutron, proton. alpha, deuteron, triton and ^{3}He used the RIPL catalog numbers 1429 [47], 5405 [47], 9600 [48], 6200 [49], 7100 [50], and 8100 [50], respectively. For deuteron break-up parametrization, the Kalbach model was used and the stripping cross section for (d,n) was calculated by using the transfer cross sections, normalized to the reaction cross section multiplied by a factor of 0.9.

4 Results and discussion

4.1 Isomeric cross-section ratios and cross section data

The measured cross sections for the ^{86}Sr(d,xn)-reactions and their uncertainties are given in Tables 2 and 3. At LBNL the data were measured from threshold up to 37 MeV and at FZJ in the energy range of 30 to 49 MeV.

All the model calculations followed the "iterative" procedure described in the paper of Sudár and Qaim [10] for the $\eta = \Theta_{eff}/\Theta_{rig}$ of the spin distribution of the level density. A similar method was used for selecting other model parameters for the calculation. Since the isomeric cross-section ratios were measured first, the η was determined for all reactions and thereafter the OMP parameters and the energy shift of the level density model were optimized. To this aim the reduced chi-squared values of the isomeric cross-

Table 3 Measured cross sections for the production of ^{86m,g}Y and ^{85m,g}Y via the ^{86}Sr+d process. Their formation from low-abundant ^{87}Sr and ^{88}Sr in the target was estimated through model calculation as <5% and <1%, respectively (see text)

Deuteron energy (MeV)	Laboratory	Measured cross section of the activation product (mb)			
		^{86m}Y	$^{86(g+xm)}$Y^a	^{85m}Y	^{85g}Y
49.1±0.3	FZJ	24 ± 3	98 ± 12	128 ± 18	63 ± 6
47.9 ± 0.3		29 ± 3	104 ± 12	118 ± 14	57 ± 5
46.7 ± 0.3		35 ± 4	134 ± 14	129 ± 18	71 ± 7
45.5 ± 0.3		39 ± 5	138 ± 15	134 ± 16	63 ± 6
44.3 ± 0.3		36 ± 4	147 ± 16	160 ± 19	76 ± 7
43.0 ± 0.4		37 ± 4	139 ± 15	163 ± 20	73 ± 7
41.7 ± 0.4		36 ± 4	141 ± 15	164 ± 20	77 ± 7
40.4 ± 0.4		46 ± 6	167 ± 20	170 ± 20	70 ± 7
38.9 ± 0.4		40 ± 4	166 ± 18	153 ± 18	71 ± 7
36.2 ± 0.4		53 ± 6	197 ± 22	209 ± 25	89 ± 8
36.0 ± 0.4		51 ± 6	204 ± 21	223 ± 26	108 ± 10
33.1 ± 0.5		60 ± 7	248 ± 26	269 ± 32	125 ± 12
32.9 ± 0.5		57 ± 6	251 ± 25	262 ± 30	138 ± 13
30.1 ± 0.5		68 ± 8	257 ± 26	204 ± 25	101 ± 10
36.9 ± 0.3	LBNL	41 ± 4	159 ± 15	158 ± 17	69 ± 7
34.1 ± 0.3		60 ± 5	236 ± 22	245 ± 27	107 ± 10
31.1 ± 0.3		63 ± 6	247 ± 23	218 ± 24	109 ± 11
28.2 ± 0.3		68 ± 6	231 ± 22	173 ± 19	86 ± 8
28.1 ± 0.4		70 ± 6	267 ± 25	165 ± 18	82 ± 8
24.6 ± 0.4		108 ± 10	332 ± 31	53 ± 6	53 ± 5
21.7 ± 0.4		216 ± 19	610 ± 57	13 ± 1.4	7.0 ± 0.6
20.9 ± 0.4		211 ± 18	619 ± 50		
18.5 ± 0.4		225 ± 20	705 ± 66		
16.9 ± 0.4		254 ± 19	856 ± 69		
15.2 ± 0.4		168 ± 12	620 ± 50		
13.4 ± 0.5		137 ± 10	536 ± 43		
11.4 ± 0.5		84 ± 6	386 ± 31		
10.5 ± 0.5		42 ± 3	207 ± 17		
10.1 ± 0.5		5 ± 0.4	25 ± 2		

^{a} Cumulative cross section of this product describes the sum of its independent formation as well as via the decay of the metastable state
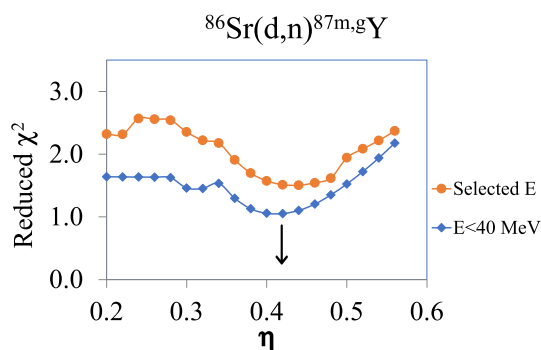
section ratios were plotted as a function of the η value for each reaction and therefrom the best fit was obtained. In general, more than 1000 calculations were done, i.e. till the parameters became practically constant. The iteration process also proved that the parameter η has only a small dependence on the other parameters. Its change was only between the final uncertainty limits during the iteration process. The reduced chi-squared values and selected measured data points are summarized in Table 4 in both TALYS and EMPIRE models. The determination and use of the η values are possible only in the TALYS code, as EMPIRE uses an approximation of the rigid momentum modified on the deformation parameters of Vigdor and Karwoski [51]. The η value of ^{87}Y has an effect on the isomeric cross-section ratio of the ^{86}Sr(d,xn)^{86,85}Y

reactions, therefore the results are presented in decreasing order of mass.

4.1.1 ^{86}Sr(d,n)^{87m}Y and ^{86}Sr(d,n)^{87g}Y processes

In graphical presentations, the results obtained at two facilities, i.e. LBNL and FZJ (which include cyclotron irradiation at Louvain-la-Neuve and some γ-counting at Brussels), are shown in the figures with different symbols. The radionuclide ^{87}Y is formed by the (d,n) reaction induced on the enriched target ^{86}Sr. This radionuclide is also formed by the (d,2n) and (d,3n) reactions on the ^{87}Sr and ^{88}Sr impurities in the enriched ^{86}Sr target. Those contributions were estimated by using experimental data on ^{nat}Sr as well as by model calculations and their values were subtracted from the total mea-
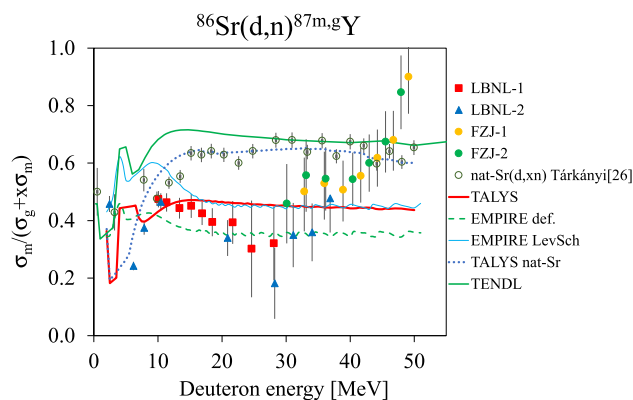
^{86}Sr(d,n)^{87m,g}Y

Fig. 1 Reduced chi-squared values of the isomeric cross-section ratio as a function of the η parameter for the ^{86}Sr(d,n)^{87m,g}Y reaction. The curve marked as "Selected E" means measured data which fall within the 3σ limit of agreement between measurement and TALYS modelling, whereas the other curve ("E< 40") contains only those points in which the incident deuteron energy is less than 40 MeV
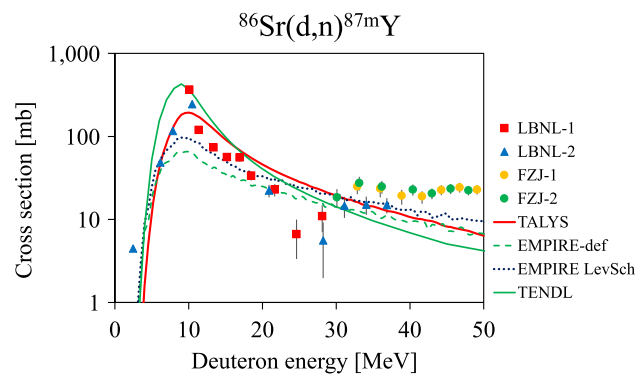
^{86}Sr(d,n)^{87m,g}Y

Fig. 2 Measured and calculated isomeric cross-section ratios as a function of the incident deuteron energy using the optimal η value of 0.44 ± 0.05 in TALYS calculation. The LBNL data point at ~ 6 MeV is rather low. The isomeric cross-section ratios based on EMPIRE calculations (see text) and the TENDL library [52] are also shown

sured value (see Sect. 2.4). A significant contribution from subsidiary reactions appeared above 10 MeV, increasing with the deuteron beam energy, reaching a value of about 70% of total formation at around 49 MeV.

For the isomeric cross-section ratio of the ^{86}Sr(d,n)^{87m,g}Y reaction, the variation of the reduced chi-squared values as a function of the η value is shown in Fig. 1. There are two curves: one contains the measured data points where the deviation of the measured and the calculated curve is less than three times the uncertainty of the measurement (3σ), and the second contains only those cases where the incident deuteron energy is less than 40 MeV, as the data from 40-49 MeV fall outside this 3σ limit. The best fit of the calculated isomeric cross-section ratio to the experimental data is $\eta = 0.44 \pm 0.05$ in both cases. The reduced χ^2 values 1.75 and 1.50 are at the minimal cases, respectively. The 3σ limit indicates which data are, from a statistical point of view, in agreement with the theory. If the excluded data are individual points, then they may indicate some experimental problem, but if the excluded points show some systematic trend then it indicates the weakness of the underlying predictive capabilities for reaction modeling theory.

Figure 2 depicts the isomeric cross-section ratios as a function of the incident energy using the optimal value of η in the TALYS calculation. The experimental data are from four sets of irradiation (indicated in the figure) and they are statistically consistent. Three model calculations are shown for the ^{86}Sr(d,n)^{87m,g}Y reaction, one with TALYS and two with EMPIRE. One of the EMPIRE calculations uses the default parameters of the code, but the second one uses the same discrete-level schema as it was used in the TALYS calculation (EMPIRE LevSch). This latter one and the TALYS calculation show very good agreement above 15 MeV. It is not clear why they are different at low energy. The default EMPIRE and TALYS calculations depict some agreement

below 10 MeV. Comparing the experimental data and the model calculation, both TALYS and EMPIRE LevSch are in good agreement with the experimental data in the energy range of 15–40 MeV. For comparison, we also inserted the TENDL data [52] which are based on TALYS calculation using default parameters. Those data are rather far from our measurements.

In the 8–15 MeV deuteron energy range, only TALYS describes the experimental data well. Above 40 MeV incident deuteron energy, there seems to be a systematic deviation of the experimental data from the isomeric cross-section ratios calculated using both TALYS and EMPIRE. The experimental isomeric cross-section ratios show an increasing trend while the calculated data represent a constant trend. Since the correction for the ^{87}Sr and ^{88}Sr is high and was based initially on the TALYS model calculation, there was some suspicion that the deviation may originate from wrong correction factors (see Sect. 2.4). Therefore, the isomeric cross-section ratios were calculated for a ^{nat}Sr target where the % of ^{88}Sr is much higher, and compared with Tárkányi et al. [26] measurements. The results are plotted in Fig. 2. It is visible that the experimental data [26] and the calculation with TALYS above 8 MeV are in good agreement. On this basis, we introduced a new correction calculation method considering the measured cross sections from natural composition of Sr. They were used to estimate cross sections from ^{88}Sr. (See the Appendix.) The correction from ^{87}Sr, however, remained unchanged. The modified correction calculation did not change the isomeric cross-section ratios. This proved that the deviation above 40 MeV does not originate from the correction method. Thus, the origin of the deviation lies in the (d,n) stripping process. In the case of the ^{nat}Sr(d,x)^{87}Y process the main component comes from the ^{88}Sr(d,3n)^{87}Y statistical reaction mechanism using the Hauser-Feshbach model which considers angular momentum conservation.

Table 4 Reduced chi-squared data while comparing the measured cross sections and calculations for the different reaction products. The (NDF $\leq 3\sigma$) column gives the number of measured cross-section data points for a reaction channel which fall within the 99.9 percent statistical probability limit of each code's model calculations, considering the uncertainties in the experimental data

Products	Type	TALYS				EMPIRE			
		$\chi^2_{red}(<3\sigma)$	NDF$(<3\sigma)$	χ^2_{red}	NDF	$\chi^2_{red}(<3\sigma)$	NDF$(<3\sigma)$	χ^2_{red}	NDF
^{87}Y	σ_m/σ_c	1.5/1.1	23/19	12	29	1.6/1.5	18/16	26.5	30
^{87}Y	σ_c	2.6	9	41	28	2.7	22	15.5	30
^{87}Y	σ_m	2.8	9	49	28	3.1	18	14.9	30
^{86}Y	σ_m/σ_c	1.2	22	3.0	26	1.5	12	29	28
^{86}Y	σ_c	1.7	15	72	27	2.0	21	58	28
^{86}Y	σ_m	2.4	15	120	26	2.4	12	60	28
^{85}Y	σ_m / σ_g	1.5	19	2.3	20	4.5	12	33	21
^{85}Y	σ_g	2.7	12	100	18	3.4	19	28	20
^{85}Y	σ_m	2.0	15	118	18	8.9	2	16	20

Fig. 3 Measured and calculated cross sections as a function of the incident deuteron energy for the ^{86}Sr(d,n)^{87m}Y reaction. The model calculations were done with the EMPIRE and TALYS codes using the optimal η value of 0.44 ± 0.05 in the TALYS calculations. The figure also shows the cross section data from the TENDL library [52]

The reduced chi-squared values while comparing the measured cross sections and model calculations are quite good for both TALYS and EMPIRE for those data in which the deviation is less than 3σ. 79% of the experimental data are below the 3σ limit compared with TALYS while the corresponding value is 60% for EMPIRE, both considered over the full deuteron energy range. The reduced chi-squared values are 1.5 and 1.6, respectively. Below the 40 MeV incident deuteron energy these data are 65%, 53%, and 1.1, 1.5, respectively. These results are summarized in Table 4.

The cross sections to produce the isomeric state ^{87m}Y ($T_{1/2}$= 13.37 h) and the results of model calculations are shown in Fig. 3. The four sets of results are in good agreement in the overlapping energy region. The cross section at 24.6 MeV is, however, too low (see discussion below for ^{87g}Y). No experimental data for the ^{86}Sr(d,n)^{87m}Y reaction are found in the literature. The TALYS code describes the experimental data quite well up to about 40 MeV but not in the

higher energy region where the theoretical value constantly decreases as compared to the experimental data. The results from the code EMPIRE seem to be good in the energy range of 20 to 40 MeV but deviate considerably from the experimental data in the range of 8 to 20 MeV and beyond 40 MeV. The experimental data above 40 MeV further strengthen the earlier hypothesis that the incorrect behaviour of the spin distribution in the description of the stripping reaction is the reason for the deviation between the models and the experiment. For comparison, we also inserted the TENDL data [52]. Our results show the improvement in the TALYS calculation with parameter adjustments. Comparing the reduced chi-squared analysis, the data of EMPIRE are better regarding the number of data points inside the 3σ limits, i.e. 60%, compared with TALYS data of 32%, but in the reduced chi-squared values, the TALYS value of 2.8 is slightly better than the 3.1 for the EMPIRE data.

The radionuclide ^{87}Y was produced via the ^{86}Sr(d,n)$^{87(g+xm)}$Y reaction, that includes 98.43% isomeric branching of ^{87m}Y. Its production cross section was measured after the complete decay of the metastable state to the ground state; the reported values thus give the cumulative cross sections.

The cumulative cross section can be expressed as a combination of the independent ground state and metastable cross section as $\sigma_{g+xm}(cum) = \left(\sigma_g + P_m \frac{\lambda_m}{\lambda_m - \lambda_g}\sigma_m\right)$ [9], where P_m is the probability of the isomeric transition to the ground state and λ_m and λ_g are the decay constants of the metastable and ground states, respectively. In case of ^{87}Y, x is 1.18. The radionuclide ^{87g}Y is also formed by two subsidiary reactions, namely ^{87}Sr(d,2n) and ^{88}Sr(d,3n). Those two reactions occur on only 1.33% abundant ^{87}Sr and 2.26% abundant ^{88}Sr in the enriched ^{86}Sr. The contributions of the subsidiary reactions were estimated from model calculations (see Sect. 2.4) and subtracted from the measured cross section of ^{87g}Y. The mea-
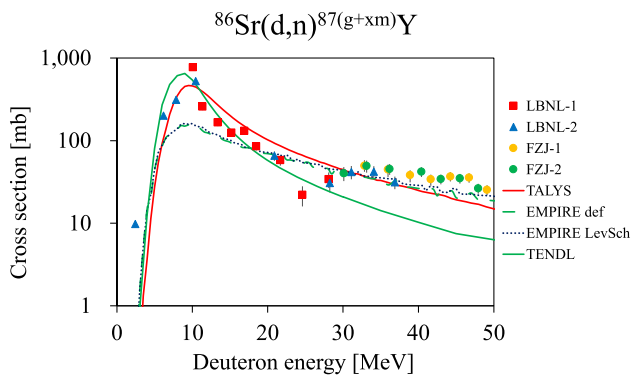
Fig. 4 Measured and calculated cross section for the $^{86}Sr(d,n)^{87g+xm}Y$ reaction as a function of the incident deuteron energy. The model calculations were done with the EMPIRE and TALYS codes using the optimal η value of 0.44 ± 0.05 in the TALYS calculations. The figure also shows the cross section data from the TENDL library [52]

sured data and the results of model calculations are shown in Fig. 4. We are reporting on the first measurements of these cross sections.

For the $^{86}Sr(d,n)^{87(g+xm)}Y$(cum) channel (Fig. 4), the results from the TALYS code describe quite well the experimental data in the energy region up to 40 MeV, except for a point at 24.6 MeV (similar to ^{87m}Y). The divergence may be due to inhomogeneity of the sample but, on the other hand, the isomeric cross-section ratio is consistent (Fig. 2), as are also the cross-section values for ^{86m}Y and ^{86g}Y (see below Figs. 7 and 8) obtained using the same sample. Thus the data points for both ^{87m}Y and ^{87g}Y at this energy appear to be authentic but the cause of the divergence remains unexplained. The EMPIRE code gives better results in the high energy region, from 20 to 50 MeV, for this reaction. From these results it is obvious that the (d,n) reaction is not described sufficiently well by any of the codes, although EMPIRE appears to give somewhat better results, possibly because of a small correction introduced recently for the deuteron break-up. As it is known, the deuteron breakup has an effect mainly on the $^{86}Sr(d,pn)^{86}Sr$ reaction channel. The $^{86}Sr(d,n)^{87}Y$ and $^{86}Sr(d,p)^{87}Sr$ reactions have a contribution from the stripping reaction, and the deviations may originate from this process. For comparison, we also inserted the TENDL data [52]. There is a visible improvement in the TALYS calculation with parameter adjustments. Comparing the reduced chi-squared values from Table 4 it is observed that the TALYS results agree better with our measurements. Only 32% of the experimental data are below the 3σ limits and the reduced chi-squared value is 2.6, while the corresponding data for EMPIRE are 73% and 2.7. These differences may come from the fact that TALYS calculations are better below 20 MeV where there are fewer measurements than above 40 MeV. Though EMPIRE describes better the high energy range; it exhibits a systematic deviation trend from the experimental

data, similar to that for the isomeric cross-section ratios. The two versions of the calculation with the EMPIRE are almost identical, independent of the used level scheme.

4.1.2 $^{86}Sr(d,2n)^{86m}Y$ and $^{86}Sr(d,2n)^{86g}Y$ processes

The radionuclide ^{86}Y has one short-lived metastable state ^{86m}Y ($T_{1/2} = 47.4$ min) and a relatively long-lived ground state ^{86g}Y($T_{1/2} = 14.74$ h). The metastable state decays 99.31% by the isomeric transition to the ground state and 0.69% by EC. The ^{86m}Y activity was measured immediately after the end of irradiation. The experimental isomeric cross-section ratios obtained in this work are shown in Fig. 5. The initial increase in the isomeric cross-section ratio with the increase in deuteron energy is attributed to the higher spin of the metastable state $(8)^+$ as compared to that of the ground state $(4)^-$ [2–4]. A comparison with the model calculation based on TALYS shows that in the energy range from 18 to 25 MeV, the model systematically underestimates the experimental data. Since in this energy range mostly the contribution of the discrete levels is dominant, this may be an indication that the level scheme is not exactly known. Beyond 25 MeV, however, the experimental and model-calculated results agree rather well. The best estimation of the η value is 0.41 ± 0.03. The analysis was done as in the case of ^{87}Y (see Fig. 6).

In Fig. 5, the calculations based on the code EMPIRE follow the shape of the experimental data, but the resulting ratios are too low in magnitude, especially above 25 MeV. For comparison, we also inserted the data from the TENDL library [52]. The deviation from our TALYS calculation indicates the importance of the level scheme of the isomers and the η parameter of the level density. Comparing the reduced chi-squared values from Table 4 shows that the data of TALYS are better in terms of the number of data points inside the 3σ lim-
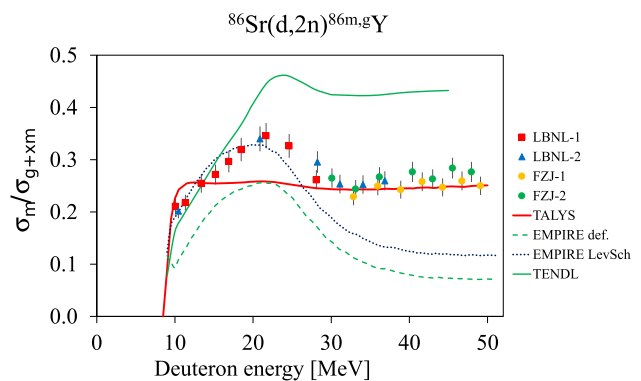
Fig. 5 Measured and calculated isomeric cross-section ratios as a function of the incident deuteron energy for the $^{86}Sr(d,2n)^{86m,g}Y$ reaction. The model calculations were done with the EMPIRE and TALYS codes using the optimal η value of 0.41 ± 0.03 in TALYS calculations. The figure also shows the isomeric cross-section data from the TENDL library [52]
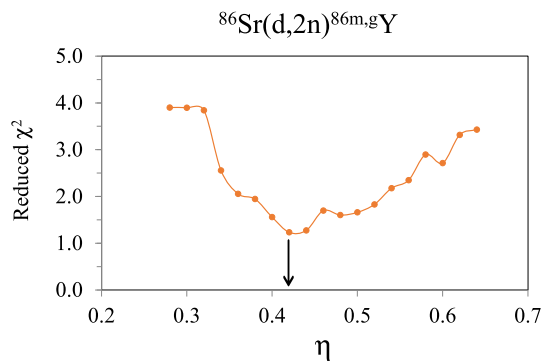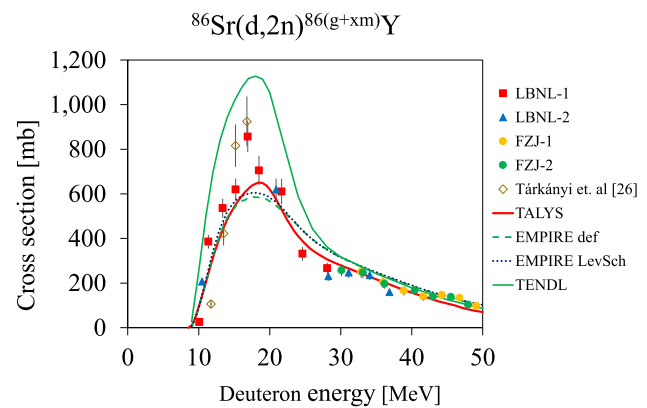
Fig. 6 Reduced chi-squared values of the isomeric cross-section ratio as a function of the η parameter for the ^{86}Sr(d,2n)^{86m,g}Y reaction
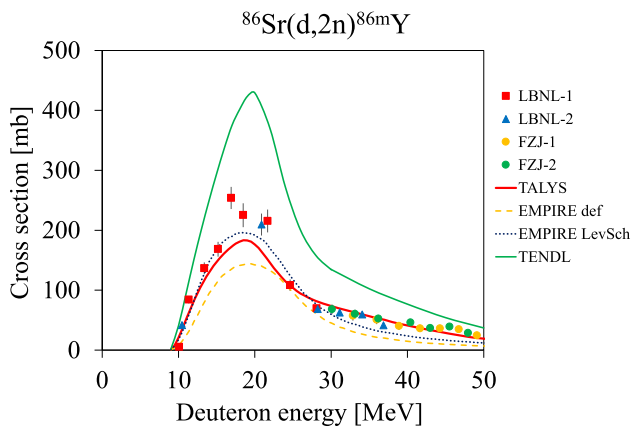
Fig. 7 Measured and calculated cross sections as a function of the incident deuteron energy for the ^{86}Sr(d,2n)^{86m}Y reaction. The model calculations were done with the EMPIRE and TALYS codes using the optimal η value of 0.41 ± 0.03 in TALYS calculations. The figure also shows the isomeric cross-section data from the TENDL library [52]

Fig. 8 Measured and calculated cross sections as a function of the incident deuteron energy for the ^{86}Sr(d,2n)$^{86(g+xm)}$Y reaction. The model calculations were done with the EMPIRE and TALYS codes using the optimal η value of 0.41 ± 0.03 in TALYS calculations. The figure also shows the isomeric cross-section data from the TENDL library [52]

its, 85% compared with EMPIRE data of 43%. Additionally, the reduced chi-squared TALYS value of 1.2 is slightly better than the 1.5 value of EMPIRE. The reduced chi-squared values for the full data set are 3 for TALYS and 29 for EMPIRE.

The measured and calculated cross sections for the ^{86}Sr(d,2n)^{86m}Y reaction are presented in Fig. 7. No experimental data exist in the literature for this reaction. Our data set consists of four independent measurements. Except for the four data points in the peak energy region near 18 MeV, the agreement between the experimental data and both the TALYS and EMPIRE-LevSch calculations is good. The EMPIRE-def. calculations, on the other hand, give lower values than the experimental data. We also inserted the TENDL data [52]. Our results show the improvement in the TALYS calculation with parameter adjustments. Comparing the reduced chi-squared values from Table 4 shows that the results of TALYS are better in terms of the number of data points inside the 3σ limits, 58% compared with 43% for EMPIRE; the reduced chi-squared value for TALYS of 2.4 is the same as the value of 2.4 of EMPIRE. The reduced

chi-squared values for the full data set are 120 for TALYS while EMPIRE has a better value of 60. Both data indicate that neither of the models can describe well the experimental data over the full energy range.

The radionuclide $^{86(g+xm)}$Y was formed via three direct deuteron-induced nuclear reactions, one on the enriched target ^{86}Sr and the other two on the impurities ^{87}Sr and ^{88}Sr. ^{86g}Y was also formed via the decay of the metastable state to the ground state. The contributions of the ^{87}Sr(d,3n)^{86g}Y and ^{88}Sr(d,4n)^{86g}Y reactions were corrected from the cross-section ratios of $\sigma(d,2n)/(\sigma(d,3n)+\sigma(d,4n))$ obtained theoretically and by considering the abundance level of ^{87}Sr (1.33%) and ^{88}Sr (2.26%) in the enriched ^{86}Sr target. In the energy range above 30 MeV, the total contribution of the (d,3n) and (d,4n) reactions was found to be small (around 2%). The cross sections measured in this work are given in Table 3 and are also shown in Fig. 8. The data measured in the two laboratories (LBNL and FZJ) agree well in the overlapping energy region. A significant part of the excitation function is fitted well by the calculation and the measured data show a smooth trend too. However, the datum at 16.9 MeV deviates from the general trend of the other experimental data (as to some extent also in the case of ^{86m}Y in Fig. 7), which is hard to explain. The isomeric cross-section ratio at this point is quite consistent with the other points. This suggests that some experimental parameters affect the cross section, which are eliminated in the isomeric cross-section ratio (e.g., particle current, mass, etc.). The particle current was the same for all energy points. This may indicate a problem with the mass of the sample (g/cm^2) used at 16.9 MeV. On the other hand, our measured value is consistent with a similar value reported by Tárkányi et al. [26] (see below).

Tárkányi et al. [26] reported ^{86g}Y production cross sections for a natural strontium target. Comparing the thresh-

old energies, it is seen that ^{86g}Y is produced mainly by the ^{86}Sr(d,2n) reaction in natural target up to 17 MeV, where the contribution from the ^{84}Sr(d,γ) reaction is considered to be negligible because the cross section of this reaction is low and the isotopic abundance of ^{84}Sr is 0.56%. Beyond 17 MeV, the (d,xn) reactions may contribute. Therefore, in the energy range below 17 MeV, a few normalized points are collected from Tárkányi et al. and are shown in Fig. 8. They are close in magnitude to our data. We also show the TALYS, EMPIRE and TENDL data in Fig. 8. The effect of parameter adjustment in our calculation is visible. The TENDL and EMPIRE reproduce the shape of the excitation function at a distance, but in TALYS the shape is missing. This is a real discrepancy, despite the latter calculation giving the best description of the experimental data.

For this reaction, a comparison of the reduced chi-squared values from Table 4 shows that the fractions of measured data points inside the 3σ limits of the TALYS and EMPIRE calculations are, 56% and 75%, respectively. The reduced chi-squared TALYS value of 1.7 is practically the same as the 2.0 value from EMPIRE. The reduced chi-squared values for the full data set are 72 for TALYS while EMPIRE has a better value of 58. Both data indicate that each model calculation can describe some parts of the excitation function well, but neither of the models can describe well the whole set of experimental data in the full energy range.

4.1.3 ^{86}Sr(d,3n)^{85m}Y and ^{86}Sr(d,3n)^{85g}Y processes

The radionuclide ^{85}Y has one metastable state ($T_{1/2} = 4.86$ h) and a ground state ($T_{1/2} = 2.68$ h). They decay independently. We could obtain independent cross-section data to produce both states. The metastable state ^{85m}Y decays 57% by positron emission and 43% by the EC. It was formed only directly via the ^{86}Sr(d,3n)^{85m}Y reaction in our investigated energy range. No data exist in the literature. The production of the ^{85g}Y occurred primarily by a single channel, i.e. ^{86}Sr(d,3n), the calculated contributions from the ^{87}Sr(d,4n) and ^{88}Sr(d,5n)-processes being negligible.

Figure 9 shows the isomeric cross-section ratios for experimental data and the nuclear reaction model calculation obtained in this work. In this case, we plotted the σ_m/σ_g values because they were directly measured; therefore their uncertainty is smaller. The highest isomeric cross-section ratio of 3.7 is found at the lowest measured energy of 21.7 MeV. The experimental ratio shows a decrease up to 28 MeV; thereafter, its trend remains experimentally constant. A good agreement in magnitude is found between the experimental data of this work and calculational results from TALYS, though it does not exactly predict the shape of the curve in this region. The EMPIRE results are, however, far from the experimental data, and neither code is able to correctly model the isomer ratio between threshold and 32 MeV.
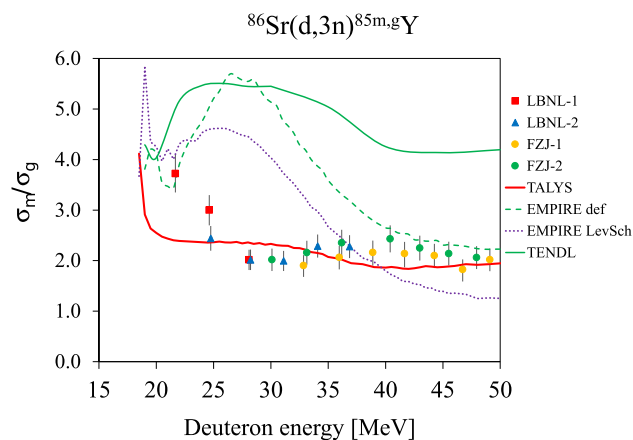
Fig. 9 Measured and calculated isomeric cross-section ratios as a function of the incident deuteron energy for the ^{86}Sr(d,3n)^{85m,g}Y reaction. The model calculations were done with the EMPIRE and TALYS codes using the optimal η value of 0.7 ± 0.1 in TALYS calculations. The figure also shows the isomeric cross-section data from the TENDL library [52]
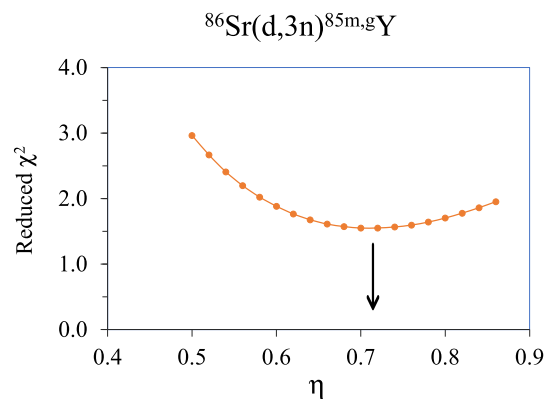

Fig. 10 Reduced chi-squared values of the isomeric cross-section ratio as a function of the η parameter for the ^{85m,g}Y reaction

The best estimation of the η value is 0.7 ± 0.1 (see Fig. 10). For comparison we also inserted the TENDL data in Fig. 9. The deviation of those data from our TALYS calculation indicates the importance of the level scheme of the isomers and the η parameter of the level density. Comparing the reduced chi-squared values of the isomeric cross-section ratios from Table 4 shows that the fraction of data points inside the 3σ limits of the TALYS is quite high at 95% while for EMPIRE it is only 57%. The reduced chi-squared value for TALYS is 1.5 while it is 4.5 for EMPIRE. The reduced chi-squared values for the full data set are 2.3 for TALYS and 33 for EMPIRE. These values indicate that TALYS can describe the experimental data in the full energy range much better than EMPIRE, although it cannot model the isomer population near the threshold correctly.

Figures 11 and 12 present the experimental cross-section data and the model calculations for the reactions ^{86}Sr(d,3n)^{85m}Y and ^{86}Sr(d,3n)^{85g}Y, respectively. The exper-
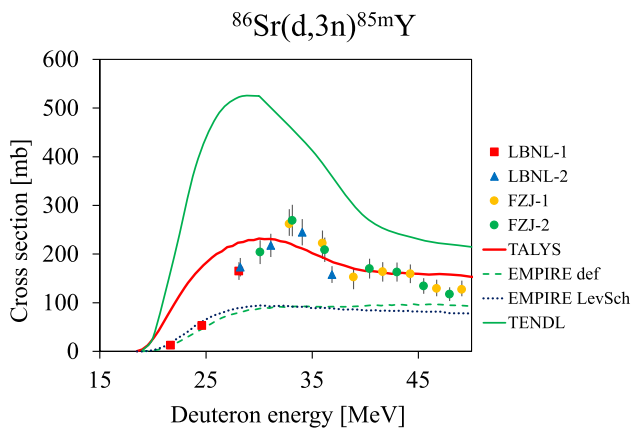
^{86}Sr(d,3n)^{85m}Y

Fig. 11 Measured and calculated cross sections as a function of the incident deuteron energy for the ^{86}Sr(d,3n)^{85m}Y reaction. The model calculations were done with the EMPIRE and TALYS codes using the optimal η value of 0.7 ± 0.1 in TALYS calculations. The figure also shows the isomeric cross-section data from the TENDL library [52]
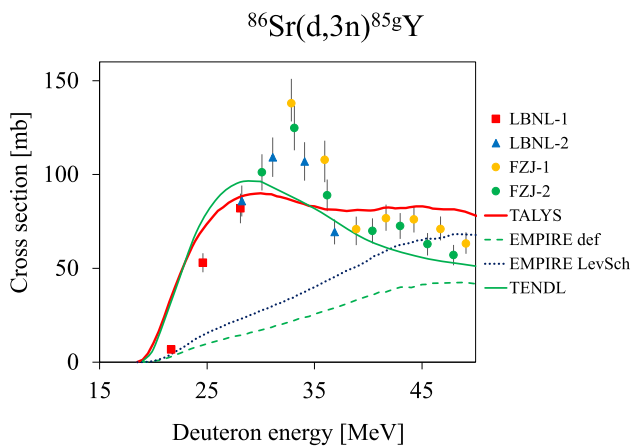
^{86}Sr(d,3n)^{85g}Y

Fig. 12 Measured and calculated cross sections as a function of the incident deuteron energy for the ^{86}Sr(d,3n)^{85g}Y reaction. The model calculations were done with the EMPIRE and TALYS codes using the optimal η value of 0.7 ± 0.1 in TALYS calculations. The figure also shows the isomeric cross-section data from the TENDL library [52]

imental data rise sharply and reach a maximum around 33 MeV and then go down sharply with the increase of energy up to 40 MeV. Above 40 MeV the change of cross section with energy is quite small. The results of the TALYS calculations are nearer to the experimental data than the EMPIRE results. The calculations with TALYS show an energy shift in the excitation function for both ^{85m}Y and ^{85g}Y production, while the EMPIRE results cannot describe the shape of the energy dependence for these reactions. Neither TALYS nor EMPIRE can describe the peak in the excitation functions near 33 MeV. One probable reason is the lack of full information on the discrete levels in ^{85}Y. We also inserted the TENDL data in Figs. 11 and 12. The improvement of the TALYS calculations with parameter adjustments is visible.

Comparing the reduced chi-squared values of the cross sections from Table 4 shows that the fraction of experimental data points inside the 3σ limits of the TALYS are quite high at 67% and 83%, while these values for EMPIRE are 95% and 10% for ^{85g}Y and ^{85m}Y, respectively. The reduced chi-squared values of TALYS for ^{85g}Y and ^{85m}Y are 2.7 and 2.0, respectively, while these values are 3.4 and 8.9 for EMPIRE. The reduced chi-squared values for the full data set are 100 and 118 for TALYS while the EMPIRE has values of 28 and 16 for ^{85g}Y and ^{85m}Y, respectively.

4.1.4 Comparative discussion of the isomeric cross-section ratios and η values

The isomeric pairs ^{85m,g}Y and ^{87m,g}Y have very similar nuclear structures. In both cases, the metastable state has a spin $9/2^+$ and the ground state $1/2^-$. In the investigated reactions the formation of the higher spin metastable state is strongly favoured. From 28 to 49.1 MeV, the isomeric cross-section ratio of ^{85m}Y/^{85g}Y (see Fig. 9) is almost constant, i.e. the ratio is independent of the incident particle energy, which differs from the ratio of ^{87m}Y/^{87g}Y, suggesting that the deuteron break-up process significantly affects the cross section of the (d,n) reaction, whereas it has only a little or no effect on the (d,3n) reaction as well as on the isomeric cross-section ratio of ^{85m}Y/^{85g}Y. The shapes of the isomeric cross-section ratios for the (d,2n) and (d,3n) reactions are similar to those for the (p,n) and (p,2n) reactions published earlier [21]. Only some energy shift is observed and the magnitude of the ratio is slightly different. Therefore, it suggests that the ratio is mainly dependent on the level structure of the respective product nucleus. Comparing the data from Table 4, the reduced chi-squared values of the isomeric cross-section ratios for the data inside the 3σ limits of TALYS calculation are all in an acceptable range (1.5, 1.2, 1.5 for ^{87}Y, ^{86}Y and ^{85}Y, respectively), while these data for EMPIRE are 1.5, 1.5, 4.5 for ^{87}Y, ^{86}Y and ^{85}Y, respectively. The reduced chi-squared values of the cross sections are always higher than the value of the isomeric cross-section ratios (except the 1.5 value for the production of $^{86(g+xm)}$Y of the EMPIRE). The analysis of the isomeric cross-section ratios in this work with deuterons has yielded η values of 0.44 ± 0.05, 0.41 ± 0.03 and 0.7 ± 0.1 for ^{87}Y, ^{86}Y and ^{85}Y, respectively. The result for ^{87}Y is new for this isotope. We previously analyzed the ^{86}Sr(p,n)^{86m,g}Y and ^{86}Sr(p,2n)^{85m,g}Y isomeric cross-section ratios in [21]. The earlier η values for ^{86}Y were 0.63 ± 0.04 based on the measurement presented in [21] and 0.69 ± 0.07 based on Levkosvskii's measurements [53]. Our new value of 0.41 ± 0.03 is in disagreement with the earlier results. It should be noted that the level scheme of ^{86}Y is incomplete and inconsistent, as discussed in [21], where attempts were made to refine it without success. Direct measurment of the branching ratios of the levels is needed. The

earlier data for the η parameter of ^{85}Y are 0.57 ± 0.06 and 0.69 ± 0.13 from [21]. These values were in good agreement within the uncertainty limits with the 0.7 ± 0.1 value obtained in the present analysis.

5 Conclusions

The cross-section data and the isomeric cross-section ratios to produce Y-isotopes via deuteron-induced reactions on ^{86}Sr were measured from the respective threshold up to 49 MeV and those results are the first ones. These data should allow calculation of the production yields of the three radionuclides ^{85m,g}Y, ^{86m,g}Y and ^{87m,g}Y as a function of deuteron energy. Therefrom, a suitable energy range for the production of ^{86g}Y could be deduced, i.e. a range where its yield would be high and the levels of the other two radioisotopes would be low.

A quantitative comparison of the two low-energy production routes of ^{86g}Y, namely (p,n) and (d,2n), can now be performed. This is presently being done and the results will be reported separately. It should then be possible to choose the more suitable production reaction at a given cyclotron. It may be reiterated that activation products of other elements (e.g. Sr, Rb) would not disturb because they can be easily removed by a chemical separation.

Both the measured cross sections and isomeric cross-section ratios were compared with the data given in the TENDL library as well as with results of nuclear model calculations based on the codes TALYS and EMPIRE, with the optimal η values used in TALYS calculations. The results show that the excitation functions of the ^{86}Sr(d,n)^{87m,g}Y process are not described satisfactorily by the three calculations, although the EMPIRE code appears to give better results. Regarding this process, more experimental information is needed, which may allow a better tuning of the optical model parameters (OMP). For the other processes, namely, ^{86}Sr(d,2n)^{86m,g}Y and ^{86}Sr(d,3n)^{85m,g}Y, however, the TALYS code seems to describe the excitation functions better. The isomeric cross-section ratios for all three reactions are reproduced partially by the TALYS code but not by EMPIRE.

Data Availability Statement This manuscript has associated data in a data repository. [Author's comment: After publication, the cross-section data are compiled by national and regional nuclear data centers and placed in the international experimental data file (EXFOR), managed by the IAEA.].

Code Availability Statement Code/Software sharing not applicable to this article as no code/software was generated or analysed during the current study.

Declarations

Conflict of interest None.

Ethics approval Not applicable.

Consent to participate All authors have consented to participate.

Consent for publication All authors approved the manuscript for publication.

Appendix A Calculation of the cross-section correction

The measured, uncorrected activity of a radioisotope is the sum of the activities produced by all isotopes of the target element by different reactions.

$$A_{unc} = A_{Sr^{86}} + A_{Sr^{87}} + A_{Sr^{88}}, \tag{A1}$$

where A is the activity and "unc" indicates the measured activity without correction, the ^{86}Sr, ^{87}Sr and ^{88}Sr indices show the contributions to the measured activity arising from reactions on each of the respective target nuclei in the sample. The activation formula for charged particle-induced reaction is:

$$A = \sigma \, c \frac{m N_A}{A_w} I_p I_\gamma \varepsilon_\gamma \left(1 - e^{-\lambda T_i}\right) e^{-\lambda T_d} \frac{\left(1 - e^{-\lambda T_c}\right)}{\lambda} \tag{A2}$$

where σ is the cross section, c is the abundance of the target nucleus in the sample, m is the mass density of the sample,

N_A is the Avogadro number, A_w is atomic mass, I_p is particle current, I_γ is the emission ratio of the detected gamma, ϵ_γ is the detector efficiency for the detected gamma, λ is the decay constant of the product, T_i is the irradiation time, T_d is the decay time, and T_c is the live counting time. It is visible that for the same product and same irradiation and counting time, the activation formula can simplify to:

$$A = \sigma \, c \, k_{case} \tag{A3}$$

where k_{case} is the remaining part of Eq. A2, which contains only common parameters for all target isotopes. Substituting this into Eq. A1 for the separated Sr isotopes sample, we get ($k_{case} = k_{sep}$):

$$\sigma^{87}_{unc} c_{Sr^{86}} k_{sep} = \sigma^{87}_{86} c_{Sr^{86}} k_{sep} + \sigma^{87}_{87} c_{Sr^{87}} k_{sep} + \sigma^{87}_{88} c_{Sr^{88}} k_{sep} \tag{A4}$$

where the upper indices of σ refer to the product Y isotope, while the lower indices refer to the target Sr isotope, e.g., σ^{87}_{88} refers to the cross section for the $^{88}Sr(d,n)^{87}Y$ reaction. The "unc" indices refer to the uncorrected data, while the "c" indices refer to the corrected cross section. The unknown cross sections were replaced by the values obtained from the model calculations, marked by "th" indices.

$$\sigma^{87}_{unc} c_{Sr^{86}} = \sigma^{87}_{86} c_{Sr^{86}} + \sigma^{87}_{87} c_{Sr^{87}} + \sigma^{87}_{88} c_{Sr^{88}} \tag{A5}$$

$$\sigma^{87c}_{86} = \sigma^{87}_{unc} - \sigma^{87th}_{87} \frac{c_{Sr^{87}}}{c_{Sr^{86}}} - \sigma^{87th}_{88} \frac{c_{Sr^{88}}}{c_{Sr^{86}}} \tag{A6}$$

It may be a better approximation if the correction is calculated by using the cross-section ratios. After multiplying out $\sigma^{87}_{86} c_{Sr^{86}}$ from Eq. A5 and simplifying with $c_{Sr^{86}}$ we get the following formula having substituted σ^{87}_{86} by σ^{87th}_{86} in the bracket:

$$\sigma^{87}_{unc} = \sigma^{87c}_{86} \left[1 + \frac{\sigma^{87th}_{87}}{\sigma^{87th}_{86}} \frac{c_{Sr^{87}}}{c_{Sr^{86}}} + \frac{\sigma^{87th}_{88}}{\sigma^{87th}_{86}} \frac{c_{Sr^{88}}}{c_{Sr^{86}}} \right] \tag{A7}$$

Due to the high correction above 40 MeV, it seems advantageous to consider the measured data for natural composition in the calculation of the correction, where the main component is the ^{88}Sr in the natural sample. Modifying the Eq. A5 for the natural composition:

$$\sigma^{87}_{nat-exp} = \sigma^{87}_{86} c_{Sr^{86}_{nat}} + \sigma^{87}_{87} c_{Sr^{87}_{nat}} + \sigma^{87}_{88} c_{Sr^{88}_{nat}} \tag{A8}$$

$$\sigma^{87c}_{88} = \frac{\sigma^{87}_{nat-exp}}{c_{Sr^{88}_{nat}}} - \sigma^{87c}_{86} \frac{c_{Sr^{87}_{nat}}}{c_{Sr^{88}_{nat}}} - \sigma^{87th}_{87} \frac{c_{Sr^{87}_{nat}}}{c_{Sr^{88}_{nat}}} \tag{A9}$$

and inserting Eq. A9 into Eq. A5.

$$\sigma^{87c}_{86} = \sigma^{87}_{unc} - \sigma^{87th}_{87} \frac{c_{Sr^{87}}}{c_{Sr^{86}}} - \left[\frac{\sigma^{87}_{nat-exp}}{c_{Sr^{88}_{nat}}} \right] \frac{c_{Sr^{88}}}{c_{Sr^{86}}}$$
$$+ \left[\sigma^{87c}_{86} \frac{c_{Sr^{87}_{nat}}}{c_{Sr^{88}_{nat}}} + \sigma^{87th}_{87} \frac{c_{Sr^{87}_{nat}}}{c_{Sr^{88}_{nat}}} \right] \frac{c_{Sr^{88}}}{c_{Sr^{86}}} \tag{A10}$$

$$\sigma^{87c}_{86} = \frac{\sigma^{87}_{unc} - \frac{\sigma^{87}_{nat-exp}}{c_{Sr^{88}_{nat}}} \frac{c_{Sr^{88}}}{c_{Sr^{86}}}}{1 - \frac{c_{Sr^{87}_{nat}}}{c_{Sr^{88}_{nat}}} \frac{c_{Sr^{88}}}{c_{Sr^{86}}}} - \sigma^{87th}_{87} \frac{\frac{c_{Sr^{87}}}{c_{Sr^{86}}} - \frac{c_{Sr^{87}_{nat}}}{c_{Sr^{88}_{nat}}} \frac{c_{SrV}}{c_{Sr^{86}}}}{1 - \frac{c_{Sr^{87}_{nat}}}{c_{Sr^{88}_{nat}}} \frac{c_{Sr^{88}}}{c_{Sr^{86}}}} \tag{A11}$$

This formula can be applied to other similar cases.

References

1. EXFOR: Experimental Nuclear Reaction Data - IAEA NDS. Database Version of 19 Oct (2022)
2. S.M. Qaim, A. Mushtaq, M. Uhl, Phys. Rev. C **38**, 645–650 (1988). https://doi.org/10.1103/PhysRevC.38.645
3. S. Sudár, S.M. Qaim, Phys. Rev. C **53**, 2885–2892 (1996). https://doi.org/10.1103/PhysRevC.53.2885
4. B. Strohmaier, M. Fassbender, S.M. Qaim, Phys. Rev. C **56**, 2654–2665 (1997). https://doi.org/10.1103/PhysRevC.56.2654
5. S. Sudár, A. Hohn, S.M. Qaim, Appl. Radiat. Isot. **52**, 937–941 (2000). https://doi.org/10.1016/S0969-8043(99)00157-8
6. K. Hilgers, S. Sudár, S.M. Qaim, Phys. Rev. C **76**, 064601 (2007). https://doi.org/10.1103/PhysRevC.76.064601
7. M.S. Uddin, B. Scholten, A. Hermanne, S. Sudár, H.H. Coenen, S.M. Qaim, Appl. Radiat. Isot. **68**, 2001–2006 (2010). https://doi.org/10.1016/j.apradiso.2010.05.002
8. M.S. Uddin, S. Sudár, S.M. Qaim, Phys. Rev. C **84**, 024605 (2011). https://doi.org/10.1103/PhysRevC.84.024605
9. S.M. Qaim, S. Sudár, B. Scholten, A.J. Koning, H.H. Coenen, Appl. Radiat. Isot. **85**, 101–113 (2014). https://doi.org/10.1016/j.apradiso.2013.10.004
10. S. Sudár, S.M. Qaim, Nucl. Phys. A **979**, 113–142 (2018). https://doi.org/10.1016/j.nuclphysa.2018.09.039
11. C. Duchemin, A. Guertin, F. Haddad, N. Michel, V. Metiviers, Phys. Med. Biol. **60**, 931–946 (2015). https://doi.org/10.1088/0031-9155/60/3/931
12. J.T. Morrell, A.S. Voyles, M.S. Basunia, J.C. Batchelder, E.F. Matthews, L.A. Bernstein, Eur. Phys. J. A **56**, 13 (2020). https://doi.org/10.1140/epja/s10050-019-00010-0
13. G. Pupillo, L. Mou, P. Martini, M. Pasquali, A. Boschi, G. Cicoria, Radiochim. Acta **108**, 593–602 (2020). https://doi.org/10.1515/ract-2019-3199
14. A.S. Voyles, A.M. Lewis, J.T. Morrell, M.S. Basunia, L.A. Bernstein, J.W. Engle, S.A. Graves, E.F. Matthews, Eur. Phys. J. A **57**, 94 (2021). https://doi.org/10.1140/epja/s10050-021-00401-2
15. M.B. Fox, A.S. Voyles, J.T. Morrell, L.A. Bernstein, J.C. Batchelder, E.R. Bernbaum, C.S. Cuttler, A.J. Koning, A.M. Lewis, D.G. Medvedev, F.M. Nortier, E.M. O'Brien, C. Vermeulen, Phys. Rev. C **104**, 064615 (2021). https://doi.org/10.1103/PhysRevC.104.064615
16. T. Sounalet, A. Guertin, F. Haddad, K. Kamalakannan, E. Nigron, Appl. Radiat. Isot. **205**, 111190 (2024). https://doi.org/10.1016/j.apradiso.2024.111190
17. G. Pupillo, L.D. Dominicis, S. Cisternino, J. Esposito, M. Campostrini, V. Rigato, F. Haddad, E. Nigron, L. Mou, J. Radioanal. Nucl Chem., in press, (2024), https://doi.org/10.1007/s10967-024-09378-w
18. M.S. Uddin, B. Scholten, M.S. Basunia, S. Sudár, S. Spellerberg, A.S. Voyles, H. Zaneb, J.T. Morrell, J. Rios, I. Spahn, L.A. Bernstein, B. Neumaier, S.M. Qaim, Radiochim. Acta **108**, 747–757 (2020). https://doi.org/10.1515/ract-2020-0021
19. H. Herzog, F. Rösch, G. Stöcklin, C. Leuders, S.M. Qaim, L.E. Feinendegen, J. Nucl. Med. **34**, 2222–2226 (1993)

20. F. Rösch, H. Herzog, S. M. Qaim, Pharmaceuticals 10, Article No. UWSP56 (pages 1-28), (2017)

21. M.S. Uddin, M.S. Basunia, S. Sudár, B. Scholten, S. Spellerberg, A.S. Voyles, J.T. Morrell, M.B. Fox, I. Spahn, O. Felden, R. Gebel, L.A. Bernstein, B. Neumaier, S.M. Qaim, Eur. Phys. J. A **58**, 67 (2022). https://doi.org/10.1140/epja/s10050-022-00714-w

22. P. Bém, E. Šimečková, M. Honusek, U. Fischer, S.P. Simakov, R.A. Forrest, M. Avrigeanu, A.C. Obreja, F.L. Roman, V. Avrigeanu, Phys. Rev. C **79**, 044610 (2009). https://doi.org/10.1103/PhysRevC.79.044610

23. M. Avrigeanu, E. Šimečková, U. Fischer, J. Mrázek, J. Novak, M. Štefánik, C. Costache, V. Avrigeanu, Phys. Rev. C **94**, 014606 (2016). https://doi.org/10.1103/PhysRevC.94.014606

24. A. Guertin, E. Nigron, M. Sitarz, C. Duchemin, F. Haddad, V. Métivier, in Proc. 15th Int. Conf. on Nuclear Reaction Mechanisms. Varenna, Italy, 11-15 June 2018, pages 355-360 (Editors: F. Cerutti, A. Ferrari, T. Kawano, F. Salvat-Pujol, P. Talou). https://doi.org/10.23727/CERN-Proceedings-2019-001

25. M.S. Uddin, M.S. Basunia, S.M. Qaim, Radiochim. Acta **109**, 727–733 (2021). https://doi.org/10.1515/ract-2021-1065

26. F. Tárkányi, A. Hermanne, F. Ditrói, S. Takács, Z. Szücs, K. Brezovcsik, Appl. Radiat. Isot. **127**, 16–25 (2017). https://doi.org/10.1016/j.apradiso.2017.04.031

27. A. Hermanne, A.V. Ignatyuk, R. Capote, B.V. Carlson, J.W. Engle, M.A. Kellett, T. Kibédi, G. Kim, F.G. Kondev, M. Hussain, O. Lebeda, A. Luca, Y. Nagai, H. Naik, A.L. Nichols, F.M. Nortier, S.V. Suryanarayana, S. Takács, F. Tárkányi, M. Verpelli, Nucl. Data Sheets **148**, 338–382 (2018). https://doi.org/10.1016/j.nds.2018.02.009

28. S. Spellerberg, B. Scholten, I. Spahn, W. Bolten, M. Holzgreve, H.H. Coenen, S.M. Qaim, Appl. Radiat. Isot. **104**, 106–112 (2015). https://doi.org/10.1016/j.apradiso.2015.06.010

29. M.S. Uddin, A.K. Chakraborty, S. Spellerberg, M.A. Shariff, S. Das, M.A. Rashid, I. Spahn, S.M. Qaim, Radiochim. Acta **104**, 305–314 (2016). https://doi.org/10.1515/ract-2015-2527

30. C.F. Williamson, J.P. Boujot, J. Picard, Tables of range and stopping power of chemical elements for charged particles of energies from 0.5 to 500 MeV. Report CEA-R 3042 (1966), https://inis.iaea.org/collection/NCLCollectionStore/_Public/35/044/35044298.pdf

31. J. Fitzgerald, JF Computing Services, 17 Chapel Road, Stanford in the Vale, Oxfordshire, SN7 8LE. Copyright © Jim Fitzgerald 1991-2016, Last updated 8th October (2016). https://www.jimfitz.co.uk/

32. S.Y.F. Chu, L.P. Ekström, R.B. Firestone, The Lund/LBNL Nuclear Data Search, Version 2.0, February (1999), http://nucleardata.nuclear.lu.se/toi/

33. A.C. Gula, E. A. McCutchan, C. J. Lister, J. P. Greene, S. Zhu, P. A. Ellison, R. J. Nickles, M. P. Carpenter, Suzanne V. Smith, and A. A. Sonzogni, Phys. Rev. C 102, 034316 (2020), https://doi.org/10.1103/PhysRevC.102.034316

34. M.S. Uddin, S.M. Qaim, B. Scholten, M.S. Basunia, L.A. Bernstein, I. Spahn, B. Neumaier, Molecules **27**, 768 (2022). https://doi.org/10.3390/molecules27030768

35. S. Sudár, "TrueCoinc", a software utility for calculation of the true coincidence correction. "Specialized software utilities for gamma ray spectrometry" 1996-2000. IAEA-TECDOC-1275. p. 37. https://www.iaea.org/publications/6359/specialised-software-utilities-for-gamma-ray-spectrometry

36. A. Negret, B. Singh, Nucl. Data Sheets **124**, 1–156 (2015). https://doi.org/10.1016/j.nds.2014.12.045

37. T.D. Johnson, W.D. Kulp, Nucl. Data Sheets **129**, 1–120 (2015). https://doi.org/10.1016/j.nds.2015.09.001

38. A.J. Koning, S. Hilaire, M.C. Duijvestijn, Proceedings of the International Conference on Nuclear Data for Science and Technology, April 22-27, 2007, Nice, France, 2007, pp. 211-214. https://doi.org/10.1051/ndata:07767

39. J. Raynal, Notes on ECIS94, CEA Saclay Reports, CEA-N-2772, (1994)

40. A.J. Koning, S. Hilarie, S. Goriely, Nucl. Phys. A **810**, 13–76 (2008). https://doi.org/10.1016/j.nuclphysa.2008.06.005

41. V. Avrigeanu, M. Avrigeanu, C. Mănăilescu, Phys. Rev. C **90**, 044612 (2014). https://doi.org/10.1103/PhysRevC.90.044612

42. J. Kopecky, M. Uhl, Phys. Rev. C **41**, 1941–1996 (1990). https://doi.org/10.1103/PhysRevC.41.1941

43. D.M. Brink, Nucl. Phys. **4**, 215–220 (1957). https://doi.org/10.1016/0029-5582(87)90021-6

44. P. Axel, Phys. Rev. **126**, 671–683 (1962). https://doi.org/10.1103/PhysRev.126.671

45. R. Capote, M. Herman, P. Oblozinsky, P. Young, S. Goriely, T. Belgya, A. Ignatyuk, A.J. Koning, S. Hilaire, V. Plujko, M. Avrigeanu, O.B.M. Chadwick, T. Fukahori, S. Kailas, J. Kopecky, V. Maslov, G. Reffo, M. Sin, E. Soukhovitskii, P. Talou, H. Yinlu, G. Zhigang, Nucl. Data Sheets **110**, 3107–3214 (2009). https://doi.org/10.1016/j.nds.2009.10.004

46. W. Dilg, W. Schantl, H. Vonach, M. Uhl, Nucl. Phys. A **217**, 269–298 (1973). https://doi.org/10.1016/0375-9474(73)90196-6

47. M. Herman, R. Capote, B.V. Carlson, P. Oblozinsky, M. Sin, A. Trkov, H. Wienke, V. Zerkin, EMPIRE: nuclear reaction model code system for data evaluation. Nucl. Data Sheets **108**, 2655–2715 (2007). https://doi.org/10.1016/j.nds.2007.11.003

48. A.J. Koning, J.P. Delaroche, Nucl. Phys. A **713**, 231–310 (2003). https://doi.org/10.1016/S0375-9474(02)01321-0

49. V. Avrigeanu, P.E. Hodgson, M. Avrigeanu, Report OUNP-94-02 (1994), Phys. Rev. C49,2136 (1994) https://doi.org/10.1103/PhysRevC.49.2136

50. H. An, C. Cai, Phys. Rev. C **73**, 054605 (2006). https://doi.org/10.1103/PhysRevC.73.054605

51. S.E. Vigdor, H.J. Karowski, Phys. Rev. C **26**, 1068 (1982). https://doi.org/10.1103/PhysRevC.26.1068

52. A.J. Koning, D. Rochman, JCh. Sublet, N. Dzysiuk, M. Fleming, S. van der Marck, TENDL: complete nuclear data library for innovative nuclear science and technology. Nuclear Data Sheets **155**, 1–55 (2019). https://doi.org/10.1016/j.nds.2019.01.002

53. V. N. Levkosvskii, Activation cross sections for nuclides of average masses (A=40-100) by protons and alpha-particles with average energies (E=10-50 MeV). Experiment and systematics. Inter-Vesy, Moscow (1992). ISBN, 5-265-02732-7